isomer distribution. For clusters with more than a few atoms, the potential energy surface is very complex, with many local minima often separated by large barriers. One consequence is that clusters need long annealing times to attain thermodynamic equilibrium. The transformation of cyclic clusters to linear clusters, for example, requires breaking a C–C bond, which implies a large barrier, especially for large cyclic clusters with little bond strain (*20*). We therefore did not expect the different isomers to be in thermodynamic equilibrium when leaving the source. Nonetheless, longer residence times in the ion source, under relatively high temperature conditions, would increase the annealing time and might shift the isomer distribution toward the thermodynamically more stable isomers.

Finally, the fact that C_n^- clusters exist in relatively large sizes suggests that neutral linear carbon clusters might also exist in this size range, because the most plausible mechanism for anion formation is electron attachment to neutral clusters. Our data do not directly address this issue, but the surprisingly large abundance of linear C_n^- species for $11 \leq n \leq 16$ supports this interpretation.

REFERENCES AND NOTES

1. P. Gerhardt, S. Loffler, K. H. Homann, *Chem. Phys. Lett.* **137**, 306 (1987).
2. P. F. Bernath, K. H. Hinkle, J. J. Keady, *Science* **244**, 562 (1989).
3. M. D. Cox, K. C. Reichmann, A. J. Kaldor, *J. Chem. Phys.* **88**, 1588 (1988).
4. P. P. Radi, T. Bunn, P. R. Kemper, M. Molchan, M. T. Bowers, *ibid.*, p. 2809.
5. S. W. McElvany, W. R. Creasy, A. O'Keefe, *ibid.* **85**, 632 (1986); S. W. McElvany, B. I. Dunlap, A. O'Keefe, *ibid.* **86**, 715 (1987); S. W. McElvany, *ibid.* **89**, 2063 (1988); *Int. J. Mass Spectrom. Ion Processes* **102**, 81 (1990); P. A. Hintz, M. B. Sowa, S. L. Anderson, *Chem. Phys. Lett.* **177**, 146 (1991).
6. K. Raghavachari and J. S. Binkley, *J. Chem. Phys.* **87**, 2191 (1987); V. Parasuk and J. Almlöf, *Chem. Phys. Lett.* **184**, 187 (1991).
7. C. Liang and H. F. Schaefer III, *J. Chem. Phys.* **93**, 8844 (1990); M. Feyereisen, M. Gutowski, J. Simons, J. Almlöf, *ibid.* **96**, 2926 (1992).
8. J. D. Watts and R. D. Barlett, *ibid.* **97**, 3445 (1992).
9. W. Weltner and R. van Zee, *Chem. Rev.* **89**, 1713 (1989).
10. S. H. Yang, C. L. Pettiette, J. Conceicao, O. Cheshnovsky, R. E. Smalley, *Chem. Phys. Lett.* **144**, 431 (1988).
11. D. W. Arnold, S. E. Bradforth, T. N. Kitsopoulos, D. E. Neumark, *J. Chem. Phys.* **95**, 8753 (1991).
12. Z. Vager *et al.*, *Z. Phys. D* **19**, 413 (1991); D. Zajfman *et al.*, *Science* **258**, 1129 (1992).
13. G. von Helden, M. T. Hsu, P. R. Kemper, M. T. Bowers, *J. Chem. Phys.* **95**, 3835 (1991).
14. _____, in *Proceedings of the SPIE Conference on Applied Spectroscopy in Materials Science II*, Los Angeles, CA, January 1992, W. G. Golden, Ed. (SPIE, Bellingham, WA, 1992), vol. 1636, pp. 182–189.
15. _____, in *Proceedings of the Symposium on Novel Forms of Carbon*, Material Research Society Conference in San Francisco, CA, May 1992, D. Cox, Ed. (Material Research Society, Pittsburgh, PA, in press).
16. P. P. Radi, G. von Helden, M. T. Hsu, P. R. Kemper, M. T. Bowers, *Int. J. Mass Spectrom. Ion Processes* **109**, 49 (1991).
17. G. von Helden, P. R. Kemper, N. G. Gotts, M. T. Bowers, unpublished results.
18. Estimated from the HOMO (highest occupied molecular orbital) orbital energies given in (*7*) by Koopmans theorem.
19. We measured reaction rate constants for both linear and cyclic C_7^+ to C_{10}^+ with a series of small molecules, and in all cases the cyclic isomer was much less reactive (*5*).
20. We carried out ab initio calculations that indicate that the energy required for ring opening is 3.75 eV and 3.5 eV for C_{10}^+ and C_{11}^+, respectively (G. von Helden and M. T. Bowers, unpublished results).
21. Support by Air Force Office of Scientific Research grant AFOSR 92-J-0021 and by NSF grant CHE91-19752 is gratefully acknowledged. G.v.H. thanks the IBM Corporation for a graduate fellowship.

28 September 1992; accepted 22 December 1992

A Mixed-Valent Polyiron Oxo Complex That Models the Biomineralization of the Ferritin Core

Kingsley L. Taft, Georgia C. Papaefthymiou, Stephen J. Lippard*

A novel polyiron oxo complex, $[Fe^{III}_4Fe^{II}_8(O)_2(OCH_3)_{18}(O_2CCH_3)_6(CH_3OH)_{4.67}]$ (1), has been prepared from ferrous acetate and lithium methoxide in methanol by slow addition of dioxygen. The three-dimensional close-packed layered structure found in 1 closely mimics that proposed for the inorganic core in the iron storage protein ferritin. The Mössbauer spectra of 1 reveal superparamagnetic relaxation at temperatures below 15 K, a property characteristic of the ferritin core. The small size and mixed-valent nature of 1 suggest that it is a reasonable model for intermediates formed in the biomineralization of iron during ferritin core formation. A related compound, with the same iron-oxygen framework found in 1 but containing only two ferric ions, has also been structurally characterized. Because the clusters exhibit properties of both discrete molecules and extended solids, they are representative of a new class of nanometer-sized compounds that bridge the molecular solid-state boundary.

Iron homeostasis is maintained in part by the iron storage protein ferritin (Ft), which is comprised of a highly symmetrical coat consisting of 24 polypeptide subunits that can encapsulate up to 4500 iron atoms in an iron oxide hydroxide core (*1–3*). This iron(III) mineral core is formed inside the preassembled protein shell upon oxidation and hydrolysis of iron(II). The structure of the iron core of Ft and the related mineral ferrihydrite is believed to consist of close-packed layers of oxygen atoms with iron occupying octahedral interstitial sites (*4–6*). Here we report the preparation and characterization of $[Fe^{III}_4Fe^{II}_8(O)_2(OCH_3)_{18}(O_2CCH_3)_6(CH_3OH)_{4.67}]$ (**1**), the structural, Mössbauer, and magnetic properties of which resemble ferrihydrite and the Ft core. Features of **1** are also realized in several other inorganic compounds, including the polyoxometalates (*7*), mixed-valent iron-containing minerals (*8*), and a variety of partially oxidized iron oxide hydroxides known as "green rusts" (*5, 6*). The characterization of **1** may help to clarify the nature of the iron core in Ft; its synthesis may serve to mimic features of the biomineralization process by which this core is deposited (*9*).

Ferrous ion dissolved in strongly basic methanol solutions reacts rapidly with excess dioxygen to give intractable yellow precipitates. In contrast, slow diffusion of dioxygen into methanol solutions of ferrous acetate and lithium methoxide yields dark blue-green rectangular crystals of **1** (*10*). The molecular structure of **1**, as determined by x-ray crystallography at 186 K, is comprised of 12 edge-shared FeO_6 octahedra (Fig. 1) (*11*). From charge and bond-distance criteria, atoms Fe(1), Fe(1)′, Fe(2), and Fe(2)′ are assigned as ferric ions. All of the iron atoms except for the two outermost ones, Fe(6) and Fe(6)′, are coordinated to the two central oxide anions. The remaining coordination sites are filled by methoxide, acetate, and methanol ligands.

Compound **1** has a distorted sodium chloride structure type, with the oxygen atoms arranged in a cubic close-packed array and the iron atoms residing in octahedral interstices (Fig. 2). Thus, the polyiron oxo molecule has a three-dimensional lattice structure of iron and oxygen atoms like that proposed for Ft and ferrihydrite. Other characterized polyiron complexes have either a layer or cluster motif, because they do not contain the μ_6-oxo ligands needed to form the lattice array of compound **1** (*12–15*). One exception is the structure that occurs in two related hexanuclear iron(III) complexes, each of which

---

K. L. Taft and S. J. Lippard, Department of Chemistry, Massachusetts Institute of Technology, Cambridge, MA 02139.
G. C. Papaefthymiou, Francis Bitter National Magnet Laboratory, Massachusetts Institute of Technology, Cambridge, MA 02139.

*To whom correspondence should be addressed.

contains a single central μ_6-oxo ligand and can be considered fragments of the lattice found in **1** (*16, 17*). The metal-oxygen framework of **1** has been observed in the early transition metal polyoxometalates (*18*), a familiar example being $[V_{10}O_{28}]^{6-}$, which contains a core of ten vanadium(V) ions joined by two central oxide anions.

The Mössbauer spectrum of **1** measured at 20 K is best fit with a single ferric and two ferrous quadrupole doublets (Fig. 3). The absorption ratio of the three components agrees with the oxidation state assignment from the structural study (Table 1). Interestingly, the Mössbauer spectrum of partially reduced horse spleen Ft also contains separate iron(II) and iron(III) quadrupole doublets (*19*). At room temperature, the three components of the Mössbauer spectrum of **1** remain distinct. At low temperatures, Mössbauer spectra of **1** exhibit superparamagnetism indicative of intramolecular magnetic ordering like that observed for Ft (*20, 21*). At 10 K, the ferric absorbance of **1** is severely broadened, whereas the ferrous subcomponents undergo intermediate spin relaxation broadening at 6 K. With decreasing temperature, magnetically split subspectra, which correspond to both ferric (Fig. 3, site I) and ferrous ions (Fig. 3, sites II and III), grow in intensity at the expense of the central, broad quadrupolar absorption. The overall magnetic splitting of all three components remains constant with temperature, a behavior consistent with superparamagnetism rather than a magnetic ordering phase transition (*21*).

The magnetic hyperfine field for the ferric subcomponent of **1** calculated from the outermost absorption features is 49.7 T (Fig. 3, site I), a value almost identical to that of 49.4 T recorded for human Ft (*21*). Based on the temperature dependence of the ferric spectral intensity, a blocking temperature (T_B) of 4 K is estimated. The ferric components of both thalassemic human spleen Ft and partially reduced Ft have a $T_B > 40$ K, presumably because of the larger crystalline regimes present in their iron cores (*19*).

Fits of the Mössbauer data of **1** have allowed two of the magnetically split ferrous subcomponents to be resolved (Fig. 3, sites II and III), with hyperfine fields of approximately 22 and 38 T and significant quadrupolar perturbations. The much reduced hyperfine fields of the ferrous sites afford proportionally

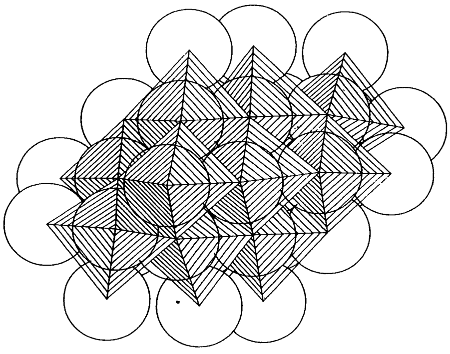

Fig. 2. View of the distorted face-centered-cubic lattice of **1** with the oxygen atoms drawn as open spheres and the 12 iron atoms as edge-shared octahedra.

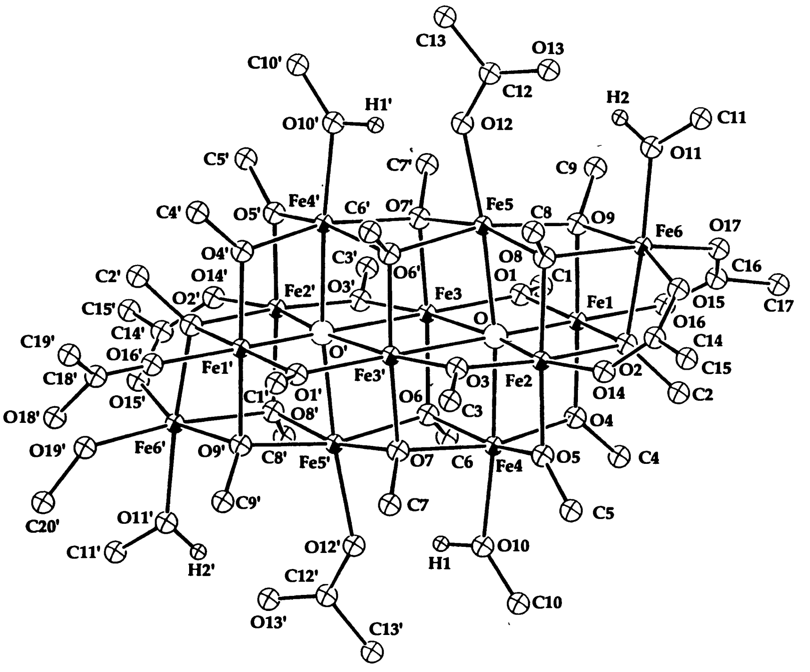

Fig. 1. Structure of $[Fe^{III}_4Fe^{II}_8(O)_2(OCH_3)_{18}(O_2CCH_3)_6(CH_3OH)_{4.67}]$ (**1**), which resides on a crystallographically imposed center of symmetry relating the primed and unprimed atoms. Iron-oxygen bond distances (Å) for the central μ_6-oxo atoms are as follows, the numbers in parentheses being the estimated standard deviations: Fe(1)–O, 2.056 (4); Fe(2)–O, 2.029 (4); Fe(3)–O, 2.409 (4); Fe(3)′–O, 2.430 (4); Fe(4)–O, 2.251 (4); and Fe(5)–O, 2.274 (4). The edge-shared Fe···Fe distances in **1** range from 3.018 (1) to 3.302 (1) Å. Hydrogen atoms of methyl groups were omitted for clarity. The four hydrogen atoms of the methanol ligands, H(1), H(1)′, H(2), and H(2)′, were located and refined. The four oxygen atoms of the two monodentate acetate ligands, O(12), O(12)′, O(13), and O(13)′, are hydrogen-bonded to the four adjacent methanol ligands. The acetate ligand bridging Fe(1) and Fe(6) was disordered and refined by using two different models. The chelating acetate O(16), C(16), C(17), and O(17) was refined at two-thirds occupancy and is shown for the unprimed atom set. The second model for the site disorder, which consists of a monodentate acetate O(16), C(18), C(19), and O(18) coordinated to Fe(1) and a methanol ligand O(19) and C(20) coordinated to Fe(6), was refined at one-third occupancy. The latter disorder model contains a hydrogen bond between O(18) and O(19) and is depicted by using the primed atom set. The additional methanol ligand O(19) and C(20) increases the molecular formula of **1** by two-thirds of a methanol, accounting for the non-integral stoichiometry.

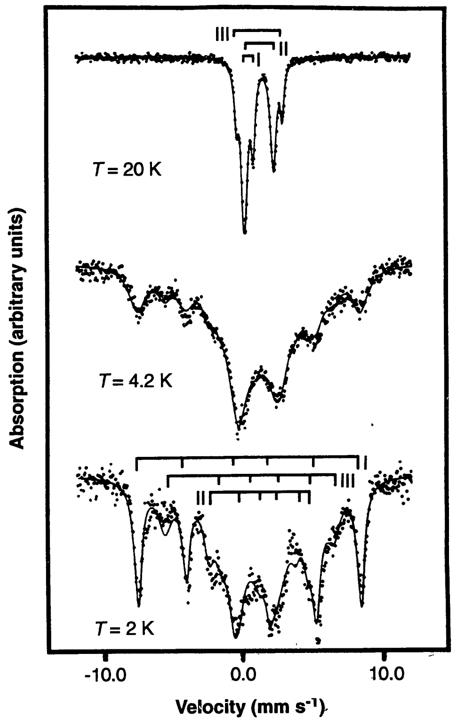

Fig. 3. Mössbauer spectra of **1** at three different temperatures. The solid lines are theoretical least squares fits to the experimental data. The bar diagrams depict spectral subcomponents associated with ferric (I) and ferrous (II and III) subsites. To obtain good fits for the low-temperature spectra (4.2 and 2 K), a broad quadrupole doublet and a background absorption envelope are superimposed over the magnetic subspectra of the three subcomponents to simulate the intermediate relaxation phenomena. Full details of the fitting procedure and parameters will be reported elsewhere (*41*).

Table 1. Comparison of Mössbauer parameters of **1** with oxidized and partially reduced Ft.

Sample	Temperature (K)	Isomer shift* (mm s^{-1})	Quadrupole splitting (mm s^{-1})	Relative intensity (%)	
				Fe(III)	Fe(II)
1 (I)†	20	0.47	0.74	29	
(II)		1.28	2.02		55
(III)		1.29	3.29		16
One-half reduced horse spleen Ft‡	100	0.47	0.67	48	
		1.25	2.88		52
Thalassemic human spleen Ft§	78	0.47	0.69	100	

*Relative to iron metal at 298 K. †I, II, and III denote iron subsites in the core of **1** (see text). ‡From (*19*). §From (*21*).

lower nuclear spin Larmor precession frequencies, which produce intermediate spin-relaxation spectral broadening down to 2 K. The ferric subsites, with a larger associated hyperfine field, have completely crossed into the slow relaxation regime at this temperature (*22*). The absence of resolvable magnetically split ferrous subcomponents in partially reduced Ft may indicate even lower ferrous hyperfine fields in the natural system or a wide distribution of ferrous sites produced upon reduction (*19*).

In the visible spectrum of **1**, there is a broad absorption centered at 710 nm that is tentatively assigned as an intervalence charge-transfer (IVCT) transition. This electronic transition, together with the room-temperature Mössbauer spectral properties discussed above, classify **1** as a type II mixed-valent complex in the Robin and Day scheme (*23*). Similar dark blue-green colors observed in mixed-valent iron minerals have been attributed to IVCT transitions, the classical example being vivianite (*8*). Intense colors also occur in hetero- and isopolyblues, a large class of reduced polyoxometalates (*7*). Partial oxidation of aqueous ferrous solutions generates green rusts, mixed-valent solutions and solids with a range of elemental compositions (*5*, *6*).

Variable-temperature magnetic susceptibility studies reveal antiferromagnetic exchange coupling among the iron atoms of **1**, a property also shared with Ft. The magnetic moment varies from 18 μ_B at 300 K to 11 μ_B at 15 K. The calculated spin-only value for four iron(III) and eight iron(II) ions is 18.2 μ_B, in accord with the assignment of redox states for the cluster. At lower temperatures, the observed magnetization is field-dependent, rendering difficult an accurate determination of the spin ground state.

Although **1** is a discrete molecule, the superparamagnetism observed in its Mössbauer spectra arises from solid-state magnetic ordering (*24*). Thus, complex **1**, which has an ellipsoidal magnetic core of approximate dimensions of 7 by 9 by 13 Å, joins a growing class of clusters in the nanometer-size regime which straddle the molecular–solid-state boundary (*25–27*). Particles ranging in size from 50 to 100 Å of the mixed-valent iron oxide magnetite (Fe_3O_4) and the iron(III) oxide maghemite (γ-Fe_2O_3) have recently been prepared in apoFt and a polymer matrix, respectively. Like compound **1**, these species exhibit superparamagnetism owing to their nanometer dimensions (*28*, *29*).

A two-electron reduced form of **1** has also been structurally characterized. This compound, **2**, has a formula of $Li_2[Fe^{III}{}_2Fe^{II}{}_{10}(O)_2(OCH_3)_{14}(O_2CCH_3)_{10}(CH_3OH)_2]$. It contains the same iron-oxygen framework found in **1** but has only two ferric ions located at positions Fe(3) and Fe(3)′ (Fig. 1), an assignment made on the basis of Fe–O bond distances. Lithium cations bridge different molecules in the crystal lattice of **2** by forming bonds to both dangling and coordinated oxygen atoms of acetate ligands. Mössbauer spectra of **2** corroborate the ratio of iron(III) and iron(II) as determined from the structural study and reveal superparamagnetism below 15 K. The presence of oxo-bridged diiron(III) moieties in both **1** and **2** suggests that cluster aggregation may require such units.

A two-stage mechanism for iron core deposition, consisting of a slow initiation and nucleation phase followed by fast growth, has been observed for Ft (*9*, *30*, *31*). The protein coat initiates mineral growth by catalyzing the oxidation of iron(II) to iron(III), and a potential ferroxidase site has recently been identified by x-ray crystallography in the H chain of Ft (*32*). The identity and location of the nucleating species within the protein cavity, however, have not yet been determined, although three glutamic acid residues located on the interior of the protein coat have been proposed for this function (*31*). A number of small iron clusters formed during Ft core growth have been observed in Mössbauer (*33*), extended x-ray absorption fine structure (EXAFS) (*34*), and electron paramagnetic resonance (EPR) studies (*35*). Core expansion proceeds during the second phase of growth on the periphery of the polyiron(III) nucleus through the binding, oxidation, and hydrolysis of ferrous ions (*36*). Compounds **1** and **2**, with oxo-bridged diiron(III) units surrounded by ferrous ions, are thus models for the first steps in the crystal growth phase, in which iron(II) binds to the iron(III) cluster prior to oxidation and hydrolysis. The further growth of **1** and **2** is prevented by the limiting dioxygen conditions and methoxide ligands because the oxide anions needed for aggregate expansion are not available. The oxo-bridged diiron(III) core is found in a number of other iron-containing metalloproteins, including hemerythrin and ribonucleotide reductase (*12*, *37*, *38*), and has been recently postulated as a product of the Ft ferroxidase center (*39*). This $\{Fe_2{}^{III}O\}^{4+}$ unit may thus be a significant component in the chemistry of Ft, serving both as an oxidation product and nucleation agent.

REFERENCES AND NOTES

1. R. R. Crichton, *Inorganic Biochemistry of Iron Metabolism* (Horwood, New York, 1991).
2. G. C. Ford *et al.*, *Philos. Trans. R. Soc. London Ser. B* **304**, 551 (1984).
3. S. Mann, J. Webb, R. J. P. Williams, Eds., *Biomineralization: Chemical and Biochemical Perspectives* (VCH Press, New York, 1989).
4. K. M. Towe and W. F. Bradley, *J. Colloid. Interface Sci.* **24**, 384 (1967).
5. J. W. Murray, in *Marine Minerals*, R. G. Burns, Ed. (Mineralogical Society of America, Washington, DC, 1979), pp. 47–98.
6. E. Murad and J. H. Johnston, in *Mössbauer Spectroscopy Applied to Inorganic Chemistry*, G. J. Long, Ed. (Plenum, New York, 1987), vol. 2, pp. 507–582.
7. M. T. Pope, *Heteropoly and Isopoly Oxometalates* (Springer-Verlag, New York, 1983).
8. R. G. Burns, in *Mixed Valency Systems: Applications in Chemistry, Physics, and Biology*, K. Prassides, Ed. (Kluwer Academic, Boston, 1991), pp. 175–199.
9. P. M. Harrison *et al.*, *Adv. Inorg. Chem.* **36**, 449 (1991).
10. To a methanol slurry of anhydrous ferrous acetate (Strem) under argon was added lithium methoxide [one equivalent per iron, prepared by careful addition of a 1.6 M butyl lithium solution in hexane (Aldrich) to anhydrous methanol], which gave a pale-green solution (~0.13 M in iron). Slow diffusion of air into a single-neck round-bottom flask containing the basic ferrous solution sealed with a rubber septum reproducibly gave dark blue-green crystals in 5 to 10% yield after 1 to 2 weeks. The solid crystalline material was isolated under argon because of its extreme air sensitivity and was washed and decanted with excess methanol to remove any yellow precipitate that formed during crystal growth.
11. Crystal data for **1**: $Fe_{12}C_{34.67}H_{90.67}O_{36.67}$, M_r = 1764.67, triclinic, space group $P\bar{1}$ (no. 2), a = 11.868 (2) Å, b = 13.309 (2) Å, c = 10.437 (2) Å, α = 100.96 (2)°, β = 95.30 (2)°, γ = 80.07 (1)°, Z = 1, V = 1591.2 (5) Å^3 (numbers in parentheses are errors in the last digit). For 4709 unique observed reflections collected at 186 K with $F^2 > 3\sigma(F^2)$, R = 0.054 and R_w = 0.071. See Fig. 1 for a description of the site disorder used in the refinement. Full details of the structural study will be reported elsewhere (K. L. Taft *et al.*, unpublished results).
12. S. J. Lippard, *Angew. Chem. Int. Ed. Engl.* **27**, 344 (1988).
13. W. Micklitz and S. J. Lippard, *J. Am. Chem. Soc.* **111**, 6856 (1989).
14. S. L. Heath and A. K. Powell, *Angew. Chem. Int. Ed. Engl.* **31**, 191 (1992).
15. K. S. Hagen, *ibid.*, p. 1010.

16. K. Hegetschweiler, H. Schmalle, H. M. Streit, W. Schneider, *Inorg. Chem.* **29**, 3625 (1990).
17. K. Hegetschweiler *et al.*, *ibid.* **31**, 1299 (1992).
18. V. W. Day and W. G. Klemperer, *Science* **228**, 533 (1985).
19. G. D. Watt, R. B. Frankel, G. C. Papaefthymiou, *Proc. Natl. Acad. Sci. U.S.A.* **82**, 3640 (1985).
20. Theoretical calculations and recent experimental observations support the onset of magnetic ordering effects in exchange-coupled atomic or molecular globular clusters containing more than ten strongly interacting spins [see (*24*)].
21. T. G. St. Pierre *et al.*, *Biochim. Biophys. Acta* **870**, 127 (1986).
22. The transition from quadrupolar to magnetically split absorption spectra at a particular iron site occurs when the Larmor precession frequency, ν_L, of the nuclear spin of the first excited state of the ^{57}Fe nucleus equals that of the spin fluctuation frequency, ν_s. The local spins in **1** are antiferromagnetically coupled with their neighbors, so they must fluctuate in unison and ν_s is the same for every iron site. Fluctuations of the total spin of the cluster between easy directions of magnetization within the nanocrystalline solid are thermally activated, so the value of ν_s decreases with temperature. Since ν_L is proportional to the local hyperfine field, H_{hf}, the transition from a paramagnetic to a magnetically split spectrum occurs at lower temperatures with smaller H_{hf}. Correspondingly, the ferrous subcomponents of **1**, with decreased H_{hf} as compared to the ferric nuclei, exhibit lower blocking temperatures.
23. M. B. Robin and P. Day, *Adv. Inorg. Chem. Radiochem.* **10**, 247 (1967).
24. G. C. Papaefthymiou, *Phys. Rev. B.* **46**, 10366 (1992), and references therein.
25. S. M. Gorun, G. C. Papaefthymiou, R. B. Frankel, S. J. Lippard, *J. Am. Chem. Soc.* **109**, 3337 (1987).
26. W. Micklitz *et al.*, manuscript in preparation.
27. J.-F. You, G. C. Papaefthymiou, R. H. Holm, *J. Am. Chem. Soc.* **114**, 2697 (1992).
28. F. C. Meldrum, B. R. Heywood, S. Mann, *Science* **257**, 522 (1992).
29. R. F. Ziolo *et al.*, *ibid.*, p. 219.
30. P. J. Artymiuk *et al.*, in *Iron Biominerals*, R. B. Frankel and R. P. Blakemore, Eds. (Plenum, New York, 1991), pp. 269–294.
31. V. J. Wade *et al.*, *J. Mol. Biol.* **221**, 1443 (1991).
32. D. M. Lawson *et al.*, *Nature* **349**, 541 (1991).
33. E. R. Bauminger, P. M. Harrison, D. Hechel, I. Nowik, A. Treffry, *Biochim. Biophys. Acta* **1118**, 48 (1991).
34. C.-Y. Yang, A. Meagher, B. H. Huynh, D. E. Sayers, E. C. Theil, *Biochemistry* **26**, 497 (1987).
35. P. M. Hanna, Y. Chen, N. D. Chasteen, *J. Biol. Chem.* **266**, 886 (1991).
36. D. Jacobs, G. D. Watt, R. B. Frankel, G. C. Papaefthymiou, *Biochemistry* **28**, 9216 (1989).
37. D. M. Kurtz, Jr., *Chem. Rev.* **90**, 585 (1990).
38. L. Que, Jr., and A. E. True, *Prog. Inorg. Chem.* **38**, 97 (1990).
39. A. Treffry, J. Hirzmann, S. J. Yewdall, P. M. Harrison, *FEBS Lett.* **302**, 108 (1992).
40. R. Fischer, *J. Appl. Crystallogr.* **18**, 258 (1985).
41. K. L. Taft *et al.*, in preparation.

42. Supported by the National Institutes of Health, the National Science Foundation, and the Office of Naval Research. K.L.T. acknowledges the National Science Foundation for a Graduate Research Fellowship. We thank H.-C. zur Loye and D. M. Giaquinta for helpful discussions and assistance in the production of Fig. 2, which was prepared by using the program STRUPLO (*40*).

20 August 1992; accepted 16 November 1992

Identification of a Second Dynamic State During Stick-Slip Motion

Hisae Yoshizawa, Patricia McGuiggan, Jacob Israelachvili*

Stick-slip, or interrupted, motion rather than smooth uninterrupted motion occurs in many different phenomena such as friction, fluid flow, material fracture and wear, sound generation, and sensory "texture." During stick-slip, a system is believed to undergo transitions between a static (solid-like) state and a kinetic (liquid-like) state. The stick-slip motion between various types of pretreated surfaces was measured, and a second, much more kinetic state that exhibits ultra-low friction was found. Transitions to and from this superkinetic state also give rise to stick-slip motion but are fundamentally different from conventional static-kinetic transitions. The results here suggest practical conditions for the control of unwanted stick-slip and the attainment of ultra-low friction.

Recent experiments (*1–4*) and computer simulations (*5–8*) have revealed that molecules at the interface between two sliding surfaces can have properties quite unlike their bulk properties. For example, simple liquids can undergo abrupt freezing-melting transitions during sliding (*2*), a phenomenon that has been shown to result in "stick-slip" friction (*6, 7*), which is the major cause of damage to moving surfaces. The ability to produce durable low-friction surfaces and lubricant fluids has become an important factor in the miniaturization of moving components in many technological devices. These include magnetic storage and recording systems (computer disk heads), miniature motors, and many aerospace components. The success of these new materials depends on the production of moving surfaces that exhibit low friction (friction coefficients below 0.01) and smooth motion with no stick-slip. Stick-slip motion, however, is a much more common phenomenon (*9, 10–18*) and is central to understanding earthquakes (*14*) and granular flows (*13, 17*).

Although the underlying physical processes are probably different in each case, most stick-slip phenomena exhibit some common features, such as an increased stick-slip frequency at higher shear rates and the disappearance of stick-slip above some critical velocity (*2, 6, 7, 9–12*). For this reason, theoretical models of these phenomena are usually similar (*6, 7, 11–14*). Thus, the existence of two states has become increasingly accepted: a "static," or solid-like, state, and a "kinetic," or fluid-like, state. In addition, the occurrence of stick-slip motion indicates that the system makes periodic transitions between these two states. Experimental and theoretical studies of liquid films (*1, 2, 6, 7*) and polymer fluids (*10, 18*) further show that the transition from stick to slip is analogous to a freezing-melting transition, which occurs when the applied shear stress reaches some critical value at which the solid-like order collapses into a disordered or liquid-like state. During the rapid slip, the elastic potential energy that was stored in the supporting material during the stick phase is transformed into kinetic energy (*9*). As slip proceeds, the two surfaces decelerate at a rate that depends on the inertial mass of the supporting material (*7*). This slowing occurs until the relative velocity of the two surfaces is small enough to allow the interfacial region to solidify again, after which the stick-slip cycle is repeated (*6*). Robbins and Thompson (*7*) have proposed that this critical velocity is given by

$$v_c \approx C\sqrt{\sigma F_s/M} \qquad (1)$$

where F_s is the static friction force, σ is a characteristic molecular or lattice dimension, M is the mass of the supporting material, or stage, and C is a constant close to 0.05. If the shearing velocity v_c is high enough, the interfacial region never solidifies, there is no stick-slip, and the two surfaces continue to move smoothly in the more fluid-like, kinetic state. The static and kinetic frictions are determined and measured solely by the properties of the shearing surfaces but only if sliding proceeds smoothly in one of those states. However, stick-slip behavior reflects transitions between any two states whose frequency, amplitude and critical velocity depend on the inertial and elastic properties of the system (moving machine component or measuring instrument). For example, in the case of interfacial sliding v_c depends directly on the inertia of the stage (Eq. 1). As a corollary to Eq. 1, Robbins and colleagues (*19*) have also found that the slip length is proportional to the inverse of the elastic stiffness of the system, which is equivalent to the constant of the spring that is used to measure the friction force in a surface forces apparatus (SFA).

A standard SFA (*20*) that was modified for shear studies (*1, 2, 15*) was used in the friction force experiments described here.

Department of Chemical and Nuclear Engineering and Materials Department, University of California, Santa Barbara, CA 93106.

*To whom correspondence should be addressed.